The behaviour of drag-reducing cationic surfactant solutions

H.-W. Bewersdorff[1]) and D. Ohlendorf[2])

[1]) Universität Dortmund, Fachbereich Chemietechnik, Dortmund, F.R.G.
[2]) Hoechst AG, Angewandte Physik, Frankfurt, F.R.G.

Abstract: The behaviour of two types of drag reducing surfactant solutions was studied in turbulent flows in pipes of different diameters. Our surfactant systems contained rod-like micelles; they consisted of equimolar mixtures of n-tetradecyltrimethylammonium bromide, n-hexadecyltrimethylammonium bromide, and sodium salicylate. The structure of the turbulence was studied using a laser-Doppler anemometer in a 50 mm pipe. In the turbulent flow regime both surfactant solutions exhibited characteristic flow regimes. These flow regimes can be influenced by changing the amount of excess salt, the surfactant concentration, or the temperature. Shear viscosity measurements in laminar pipe and Couette flows show the occurrence of the so-called shear-induced state, where the viscosity increases and the surfactant solution becomes viscoelastic. The shape of the turbulent velocity profile depends on the flow regime. In the turbulent flow regime at low Reynolds numbers, velocity profiles similar to those observed for dilute polymer solutions are found, whereas at maximum drag reduction conditions more "S-shaped" profiles that show deviations from a logarithmic profile occur. An attempt is made to explain the drag reduction by rod-like micelles by combining the results of the rheological and the turbulence structure measurements.

Key words: Drag reduction, shear viscosity, surfactant, turbulence, velocity profile.

1. Introduction

Most of the published work in the field of drag reduction by additives deals with polymeric additives. Nevertheless, drag reduction in turbulent flows can also be obtained by the addition of fibres or surfactants. Although surfactants were used in one of the earliest experiments where drag reduction was reported [1], relatively little work has been published in the field of drag reduction by surfactants in comparison to other types of additives. A review of drag reduction with special reference to surfactant drag reduction was published in 1984 by Shenoy [2].

Drag reduction has great potential practical applications in view of the possible large reduction of energy losses due to turbulent friction. A review of current and possible future applications was published by Sellin et al. [3]. The main current application of drag reduction is the increase in flow rate in crude-oil pipelines by the addition of polymers [4]. Furthermore, polymeric additives prevent flooding in sewers by increasing the flow rate during times of overloading by

heavy rain [5]. A problem of using polymeric additives in closed circuits is degradation, i.e., polymers lose their drag-reducing properties with the number of passes in a closed circuit due to a change of their molecular parameters. However, for practical applications in closed circuits, like central-heating systems, cooling circuits and air-conditioning systems, the use of drag-reducing surfactants may prevent these degradation problems. Several authors have found that no degradation occurred over long time periods in surfactant solutions [6–13].

"Surfactant" is a convenient abbreviation of "surface-active agent". Among the surfactants used for drag reduction one has to differentiate between nonionic, anionic, and cationic surfactants. The disadvantage of anionic surfactants, which are mainly salts of fatty acids, is that they form insoluble salts with the calcium and magnesium ions present in tap and sea water [2, 14, 15]. This disadvantage is avoided by a combination of the cationic surfactant hexadecyltrimethylammonium bromide, often called CTAB, and 1-naphthol

[8, 11, 12, 15, 16]. Mixtures of 1-naphthol with other cationic surfactants based on quaternary ammonium salts have been described [11, 17, 18].

It has been shown that these and other cationic surfactants in combination with a variety of different organic ions, e.g., sodium salicylate, can be used as drag reducing agents [7, 9, 13, 19–23] in water. These surfactant systems give rise to rod-like micelles. These are formed by single surfactant molecules if the concentration exceeds a characteristic surfactant concentration, c_t, which depends strongly on the temperature [7, 26, 27]. Drag reduction occurs only if rod-like micelles are present in the solution [7, 23]. The length of the rods and the degree of drag reduction both increase with increasing surfactant concentration. In the concentration range for drag reduction, typically 500–2000 ppm by weight, the length of the rod-like micelles is less than 80 nm. In such surfactant solutions at rest, the rods can rotate freely without interfering with each other [7]. It was Savins who first recognized that drag-reducing surfactant solutions show a viscoelastic flow behaviour [10].

Shear viscosity measurements in laminar pipe and Couette flows show that these dilute surfactant solutions behave like normal Newtonian fluids at low shear rates. At shear rates above a critical value, however, the viscosity suddenly increases due to the formation of a shear induced state (SIS) [7, 13, 23, 25, 27–30]. The critical shear rate and the increase in viscosity depend not only on the temperature and surfactant concentration, but also on the geometry of the measuring equipment, e.g., the slit width of the Couette viscometer [7]. The formation of the SIS is accompanied by a marked flow birefringence. Flow birefringence measurements show that in the SIS the rods are completely aligned in the direction of the flow [24, 25]. The origin of the SIS is not yet fully understood. Two models have been discussed: coalescence of the rod-like micelles to form very long flexible rods that act like high molecular polymers, or the build-up of ordered structures of individual rods by cooperative electrostatic interaction [7, 24, 25, 29, 30].

The turbulent friction behaviour of drag reducing surfactant solutions is characterized by the critical wall-shear stress. Beyond this critical wall-shear stress a reversible loss of drag reduction is observed, i.e., drag reduction is recovered when the wall-shear stress again falls below the critical value [7, 9, 10, 11, 16, 32]. The critical wall-shear stress is independent

of the pipe diameter [6, 11, 32, 33] and can be increased by increasing the concentration [9, 15, 33]. The turbulent friction behaviour depends on the size, number, and surface charge of the micelles [7, 23]. Even in pipes of larger diameters Virk's [34] maximum drag reduction asymptote can be approached [7, 9, 12, 13, 32]. Recent small angle neutron scattering experiments [35] in a turbulent channel flow demonstrated that micelles are not destroyed by excess critical wall-shear stress, but that their orientation and superstructures break down instead. This agrees with [7] which showed that the time constants involved in the formation of rod-like micelles are on the order of 10^3–10^4 s for the surfactants used in [35].

Velocity profile measurements in turbulent flows of drag reducing surfactant solutions have been carried out in both channel [36–38] and pipe flows [13]. The experimental results (as shown in Figures 10–15 of this work) show that the dimensionless velocity profile at the end of the viscous sublayer, which seems to be unchanged, follows Virk's [34] ultimate profile in the buffer zone. In the core region the velocity profiles are sometimes parallel to the Newtonian core region as is found for drag-reducing dilute polymeric solutions. They sometimes have an increased slope in the core region that indicates a changed turbulence structure in this region. In the case of Virk's [34] maximum drag reduction the velocity profiles in the buffer region are S-shaped, i.e., they deviate from Virk's logarithmic ultimate profile at smaller wall distances to lower, in the medium range to higher, and at larger wall distances to lower dimensionless velocity values. Therefore the shape of the dimensionless velocity profiles at maximum drag-reduction conditions is more similar to a laminar profile than to a turbulent logarithmic profile. The maximum of the axial turbulence intensity, normalized by the friction velocity, is shifted towards the centre of the channel or pipe in comparison with a Newtonian fluid. It seems to decrease in channel flows and to increase in pipe flows.

In the present article the experimental results of the rheological properties, the friction behaviour and the turbulence structure measurements of two cationic drag-reducing surfactant solutions are summarized. Special attention is also given to the influence of temperature and concentration on the micellar properties and flow behaviour. A deeper knowledge of the interaction between micelles and turbulence structure which leads to drag reduction is sought.

2. Experimental

2.1. Sample material

Two cationic surfactants were investigated. Equimolar mixtures of the cationic surfactants n-tetradecyltrimethylammonium bromide, C_{14}TABr, or n-hexadecyltrimethylammonium bromide, C_{16}TABr, with sodium salicylate (NaSal) were used. These mixtures were added to the desired amount of tap water and pumped around in a closed-circuit flow system for approximately three days, heating up to a maximum temperature of 30 °C. Thus the surfactant solutions n-tetradecyltrimethylammonium salicylate (C_{14}TASal) and hexadecyltrimethylammonium salicylate (C_{16}TASal) were obtained in a thermodynamic state of equilibrium that contained an equimolar amount of the salt NaBr.

2.2 Experimental set up

The lengths of the rod-like micelles were determined by electrical birefringence measurements; the apparatus used and the evaluation of the data were similar to those described in [39, 40].

The flow curves of the surfactant solutions were investigated in Couette viscometers, i.e., at low shear rates in the Low Shear 2 and 100 viscometer by Contraves and at high shear rates in the Rotovisko RV 2 viscometer by Haake. The measuring systems used were system 1 for the Low Shear 2 and 100 (gap widths 0.5 mm) and NV for the Rotovisko (double gap widths 0.4 and 0.5 mm). In addition a capillary viscometer ($d = 2$ mm, $l = 13.7$ m) described in detail in [7] was used.

The friction behaviour data were obtained in three different flow systems with pipe diameters of 6 mm, 30 mm, and 50 mm. The fluid was continuously pumped around in these closed systems. The flow rates were recorded by inductive flowmeters (Fisher & Porter D10 DK 1425), the temperatures by resistance thermometers, and the pressure drops by pressure transducers placed between pressure taps spaced 1 or 2 m apart. A sufficiently long entrance length of $l/d \approx 280$ was provided to ensure a fully developed turbulent flow in the measuring section, since the Newtonian entrance length of $l/d = 50$ is increased in the flow of drag-reducing polymer solutions. The axial velocity component was measured using a laser-Doppler-anemometer (LDA) supplied by DISA and operated in the backscattering mode in the 50 mm pipe 280 diameters beyond

the entrance of the pipe. To avoid distortion of the laser beam due to the curvature of the pipe, a flat window was inserted in the pipe and the velocity data measured in the opposite part of the axial symmetric velocity profile. The measuring volume was 0.8 mm in length and 0.05 mm in diameter with a fringe spacing of 5 μm. A computer collected 14000 data of the momentary axial velocity at each measuring point, measurements being taken every 20 ms. For the measurements of the autocorrelation function and the energy spectra the data were collected with a sample frequency of 500 Hz. The measuring volume could be traversed by focussing the front lense of the LDA-system. A more detailed description of the LDA-system used can be found in [41].

3. Experimental results

3.0 Influence of salt on surfactant systems

All surfactant solutions used for drag reduction and LDA measurements were prepared by dissolving the proper amounts of equimolar mixtures of the salts C_nTABr and NaSal in tap water. Apart from the surfactant C_nTABr the solutions investigated always contained an equimolar amount of NaBr and slightly varying amounts of other electrolytes. Additional electrolytes greatly influence the physico-chemical and rheological properties of micellar systems [23, 42, 43].

Excess salt shifts the characteristic concentration of the build-up of rod-like micelles, c_t, to lower values and consequently the lengths of the rods start to increase [23, 42]. Figure 1 shows the change of the rod length in a C_{14}TASal solution as a function of both the temperature and the water used for the experiments. The lengths of the rods increase with increasing salt concentration and decrease with temperature. Elsewhere it is demonstrated that the kinetics of the micellar system are influenced very dramatically by excess salt [42, 45]. Consequently, the laminar and turbulent flow behaviours of the surfactant solution are changed similarly by the addition of salt and by an increase in temperature (compare the results in chapter 3.1 and 3.2) [45]. Nevertheless, all the results of this work are valid because the principal laminar and turbulent flow behaviours of the surfactant systems used are still the same.

3.1 Shear viscosity measurements

As mentioned in chapter 2 the flow curves of the surfactant solutions were investigated in Couette viscometers and in a capillary viscometer. Figure 2 shows a plot of the shear viscosity versus shear rate for equimolar mixtures of C_nTASal and NaBr in tap water. The C_{14}TASal solution behaves like a Newtonian fluid
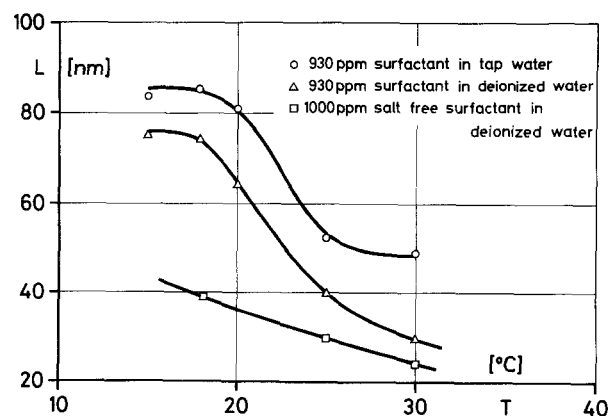
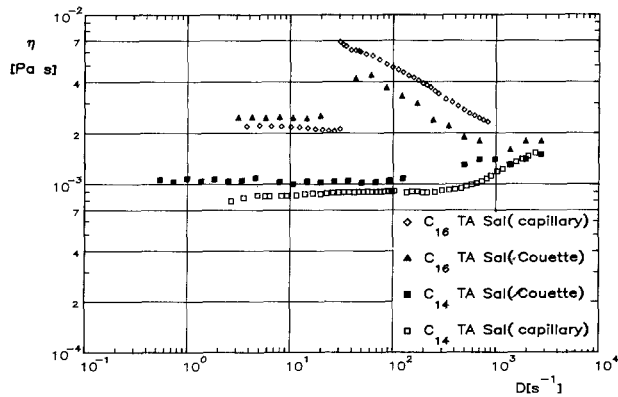Fig. 1. Length of the rods of a solution of C_{14}TASal

Fig. 2. Shear viscosity of a $C_{14}TASal$- or $C_{16}TASal$ solution in tap water at $T = 22.5\,°C$ and $c = 930\,ppm$

Fig. 4. Shear viscosity at various temperatures of pure $C_{14}TASal$ solution (without NaBr) in de-ionized water at $c = 1000\,ppm$

at low shear rates. Only for $D > 200\,s^{-1}$ can a slight increase of the viscosity be observed. The $C_{16}TASal$ solution shows a more complex rheological behaviour. In the shear range $D = 20$–$50\,s^{-1}$ the viscosity suddenly increases by a factor of 2.5 due to the formation of the shear-induced state (SIS) [7,13,23,25,27–30,31]. It was impossible to estimate the shear viscosity in this range in the Low Shear Viscometer because the cylinder moved elliptically in the gap due to its non-compulsorily centred cylinder so that no steady values of torque could be obtained. Furthermore, in [7] a shear viscosity depending on the gap width of the viscometer was found in this range. At higher shear rates the viscosity declines with increasing shear rate for the $C_{16}TASal$ solution.

To demonstrate the influence of the additional salt present in tap water, Fig. 3 shows viscosity data of the $C_{14}TASal$ solution at various temperatures in de-
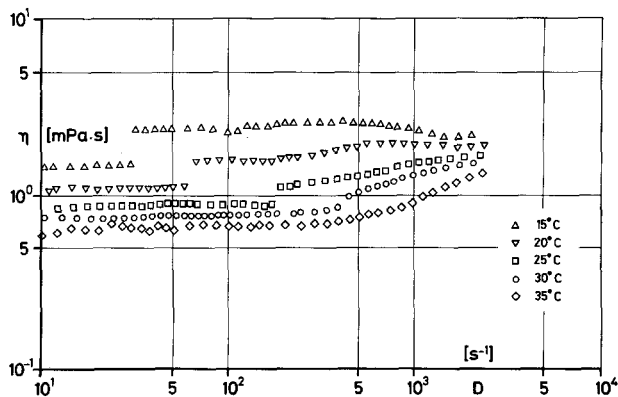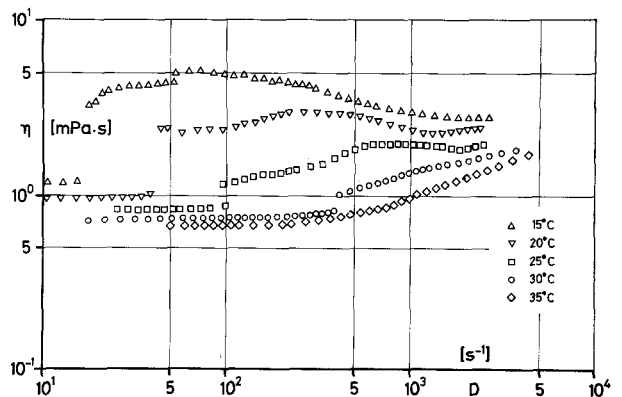
ionized water. In de-ionized water the SIS also occurs in the $C_{14}TASal$ solution. However, the magnitude of the increase in the shear viscosity at the critical shear rate, where the SIS occurs, decreases with increasing temperature. At higher temperatures the flow curves are steadier and the viscosity increases only at higher shear rates. Figure 3 shows how the occurrence of the SIS is shifted to higher shear rates with increasing temperature.

Figure 4 displays shear viscosities measured in laminar pipe flow as a function of shear rate and temperature for a 1000 ppm solution of the pure surfactant $C_{14}TASal$ in de-ionized water. A comparison of Figs. 2–4 demonstrates that with an increasing amount of excess salt the critical shear gradient $\dot{\gamma}_t$ for the build up of the SIS is shifted to higher shear rates and the increase in shear viscosity at $\dot{\gamma}_t$ decreases. As mentioned already in chapter 3.0 the addition of electrolytes to surfactant solutions influences the shear viscosity in a way similar to an increase in temperature.

3.2 Friction behaviour

The friction behaviour of the surfactant solution was determined by measurements of the pressure drop and the flow rate in pipes of different diameters. In the plots of the friction behaviour the friction factor is defined by

$$f = \frac{\Delta p\, d}{2\, l \varrho w^2} \tag{1}$$

where $\Delta p / l$ indicates the pressure drop per unit length, d the diameter of the pipe, ϱ the density of the fluid,

Fig. 3. Shear viscosity at various temperatures of a $C_{14}TASal$ solution in de-ionized water at $c = 930\,ppm$

and w the bulk velocity. The Reynolds number is defined by

$$Re = \frac{w\,d}{v} \tag{2}$$

where v is the kinematic viscosity of the solvent. In studies of the friction behaviour of drag-reducing fluids it is convenient to use the solvent viscosity instead of the solution viscosity, since, according to Virk [34], the shear-thinning behaviour of dilute polymeric solutions has little effect on gross flows. Whether this convention is suitable for surfactant solutions showing a different rheological behaviour compared to dilute polymer solutions (see last section) will be discussed later. The advantage of this convention is that whenever shear-induced states have an influence on the (turbulent) friction behaviour of surfactant solutions an increase in the friction factor should occur at a certain Reynolds number. In addition, this convention permits the checking of the empirical friction law of maximum drag reduction [34]

$$\frac{l}{\sqrt{f}} = 19 \log_{10} (Re \sqrt{f}) - 32.4 \;, \tag{3}$$

which seems to limit the maximum attainable drag reduction.

In Fig. 5 the friction factor f of the C_{14} TASal solution in tap water in equimolar mixture with NaBr in a 6 mm pipe is plotted versus the Reynolds number for different temperatures. In the laminar-flow regime all friction factors of the surfactant solution lie above those determined by the equation $f = 16/Re$ which results
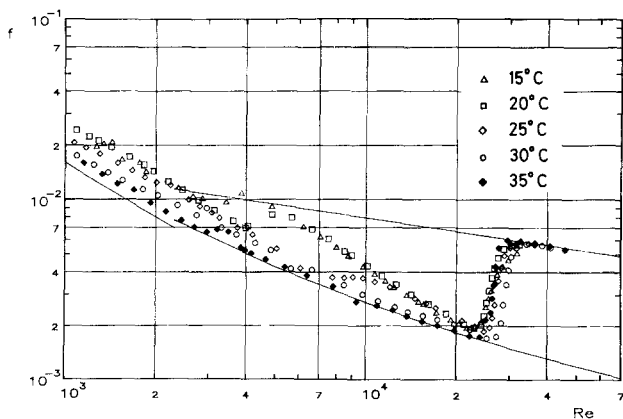
from Hagen-Poiseuille's law. The drag-reduction regime is limited by the Prandtl-Kármán law for a Newtonian fluid

$$\frac{l}{\sqrt{f}} = 4 \log_{10} (Re \sqrt{f}) - 0.4 \tag{4}$$

and by Virk's maximum drag reduction asymptote, Eq. (3).

The friction behaviour in the turbulent-flow regime depends strongly on the temperature. At lower temperatures the friction factor slightly increases at the end of the laminar-flow regime and approaches the Prandtl-Kármán law for the turbulent flow of a Newtonian fluid. At these lower temperatures the surfactant solution shows an onset behaviour as observed in the flow of dilute polymer solutions [34], i.e., drag reduction in turbulent flow occurs when a critical wall-shear stress or better a critical value of u_τ^2/v is exceeded. At higher temperatures this onset phenomenon disappears. However, a remnant of this behaviour remains in the form of a bump in the curves for the higher temperatures. With increasing temperature the friction factors in the turbulent flow regime follow Virk's maximum drag-reduction asymptote, Eq. (3), until finally the drag-reduction vanishes at higher Reynolds numbers, where it exceeds the critical wall-shear stress. This critical wall-shear stress decreases with increasing temperature from $\tau_w = 16.8\ Pa$ at 15 °C to $\tau_w = 6.2\ Pa$ at 35 °C.

The C_{14} TASal solution in equimolar mixture with the salt NaBr in de-ionized water exhibits a friction behaviour as shown in Figure 6. Due to the higher shear viscosities (see Fig. 2) in comparison with the
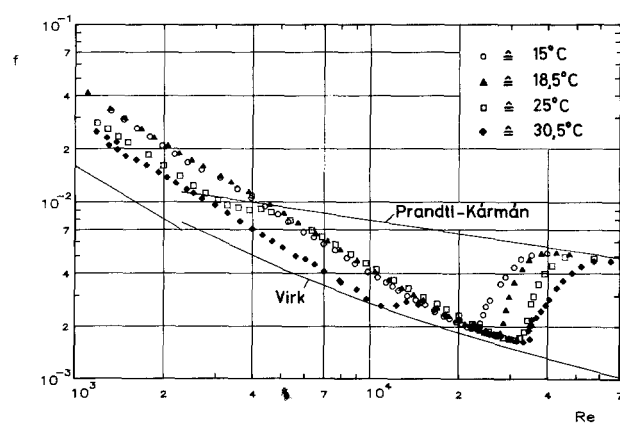

Fig. 5. Friction behaviour of a C_{14} TASal solution in tap water for various temperatures in a 6 mm pipe at $c = 930$ ppm

Fig. 6. Friction behaviour of a C_{14} TASal solution in de-ionized water for various temperatures in a 6 mm pipe at $c = 930$ ppm

C_{14}TASal solution in the laminar-flow region higher values of the friction factor are obtained in tap water. At lower temperatures (15 °C and 18 °C) the friction factor decreases linearly with the Reynolds number until the critical wall-shear stress is reached and a breakdown of the drag reduction occurs. In the medium temperature range (25 °C) a bump in the friction behaviour is observed like that for the C_{14}TASal solution in tap water, whereas at the higher temperatures the friction factors decrease linearly until Virk's [34] maximum drag-reduction asymptote is approached. A comparison of the shape of the flow curves, f versus Re, in the Figs. 5 and 6 demonstrates, that the additional electrolytes included in the tap water have the same effect on the turbulent pipe flow behaviour of the surfactant solution as an increase in temperature. The shapes of the flow curves, f versus Re, for 25 °C (18-20 °C) for tap water in Fig. 5 are quite similar to the flow curves for 30 °C (25 °C) for de-ionized water in Fig. 6.

In pipes of different diameters (Fig. 7) different flow regimes can be detected in the friction behaviour of the C_{14}TASal solution in tap water. These flow regimes occur in each pipe diameter at different Reynolds numbers. The limits of the flow regimes are shifted to higher Reynolds numbers with increasing pipe diameter. At lower Reynolds numbers in the turbulent flow regime (Fig. 8) the friction factor falls linearly (region 1) to approach Virk's maximum drag-reduction asymptote (region 2). At higher Reynolds numbers a flow region (region 3) occurs in which the friction factor is nearly constant. A further increase in the Reynolds number results in a further decrease of the friction fac-
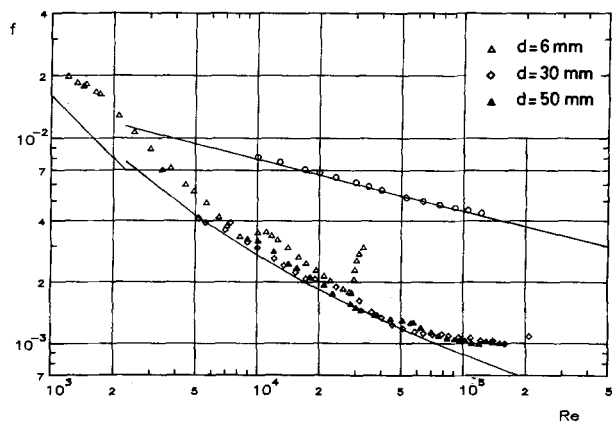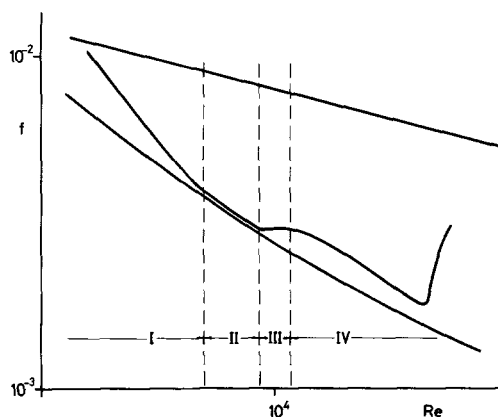

Fig. 8. Regions in the friction behaviour of the C_{14}TASal solution

tor (region 4) until the critical wall-shear stress is exceeded and the drag-reducing properties start to breakdown. Due to the limited range of measurement all these regions were only detectable in the 6 mm pipe. The same different flow regimes were also found in [7, 9] for saltfree solutions of C_{14}TASal and C_{16}TASal in de-ionized water at different temperatures. The bump in the flow curves, the limit between region 2 and 3, occurs at wall-shear gradients of about $\dot{y} = 2700\,s^{-1}$ for all pipe diameters.

The friction behaviour of the C_{16}TASal solution in equimolar mixture with the salt NaBr (Fig. 9) which was measured in the 6 and in the 50 mm pipe indicates the influence of the increased shear viscosity (see Fig. 2). At low Reynolds numbers the friction factor decreases with a highly negative slope and crosses the
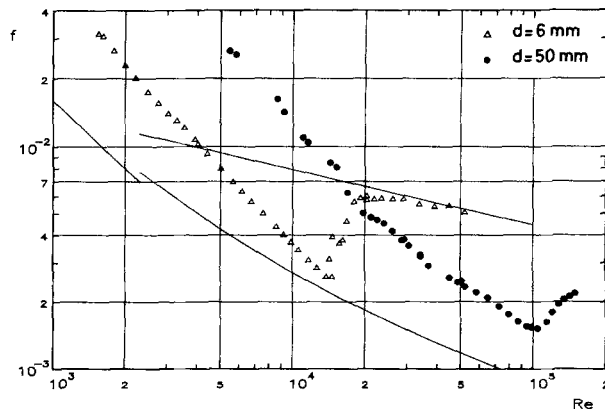

Fig. 7. Friction behaviour of a C_{14}TASal solution in tap water at $T = 23$ °C in pipes of different diameters at $c = 930$ ppm. The open circles are solvent data

Fig. 9. Friction behaviour of a C_{16}TASal solution in tap water at $T = 25$ °C in pipes of different diameters at $c = 830$ ppm

Prandtl-Kármán line for Newtonian fluids. The critical wall-shear stress, where the drag-reducing properties start to break down lies at 5.8 *Pa* in the 6 mm and at 5.3 *Pa* in the 50 mm pipe. For this solution, Virk's maximum drag-reduction asymptote could not be reached. This is understandable because in the whole shear range the solution viscosity is increased in comparison to that of the solvent, and the Reynolds number is based on the solvent viscosity. The C_{16}TASal solutions exhibit a friction behaviour [9] at higher temperatures (50–65 °C) which is similar to that found in the present work on the C_{14}TASal solution. However, at these temperatures the flow curves, shear viscosity versus shear gradient, become steadier and the occurence of the shear-induced state is shifted to higher shear rates [7].

The LDA measurements of the turbulence structure were carried out in a closed circuit of a 50 mm pipe. The solutions were circulated in the closed loops for about six weeks. During this time no degradation occurred, but a slight reduction of the surfactant concentration in the closed circuit was found. For example, the initial concentration of the C_{14}TASal solution was 930 ppm by weight. Chemical analysis showed 927 ppm. Six weeks later, at the end of series of LDA measurements, it had fallen down to 864 ppm determined by chemical analysis. This effect was observed in all long-term experiments with surfactant solutions in a closed circuit. It is therefore assumed that the observed reduction of the surfactant concentration is due to an adhesion of surfactant molecules on the inner walls of the experimental set up.

Furthermore, the colour of the surfactant solutions, initially colourless, changed as the experiments progressed. They first turned yellow, later on brown, and lastly black. A change in colour of a surfactant solution C_{16}TABr in equimolar mixture with α-Naphthol, was also reported in [15] where a slow turn to brown was observed. We found that the black colour of the surfactant solutions was caused by an interaction between the surfactant solution and the stator of the Mohno pump made of Perbunan. Small carbon particles were released by the stator, which therefore was abraded very fast. This degree of colouring to black was accompanied by an increasing absorption of the light of the laser beam of the LDA. In about six weeks the solution changed its colour to totally black and had to be replaced by a new one due to the poor quality of the LDA-signals. Surprisingly no change of the friction behaviour could be observed during the six weeks of each series of LDA-measurements.

3.3 Velocity profile measurements

Turbulent velocity profiles are usually plotted in dimensionless coordinates where a dimensionless velocity

$$U^+ = \frac{U}{u_\tau} \tag{5}$$

and a dimensionless wall distance

$$y^+ = \frac{y\,u_\tau}{v} \tag{6}$$

are used. In these two equations U means the time averaged local velocity, y the wall distance, v the kinematic viscosity, and u_τ the friction velocity defined by

$$u_\tau = \sqrt{\frac{\tau_w}{\varrho}} \tag{7}$$

where τ_w is the wall shear stress and ϱ the density of the fluid. In this way the universal velocity profile is obtained for a Newtonian fluid which mainly shows two regions, the viscous sublayer at the wall

$$U^+ = y^+ \tag{8}$$

and the turbulent core

$$U^+ = A \ln y^+ + B \tag{9}$$

where $A = 2.5$ and $B = 5.5$. Between these two regions a small transition region exists, often called a buffer zone. It has been shown in drag-reducing dilute polymer solutions that the viscous sublayer seems to be unchanged whereas the velocity profile in the buffer zone follows Virk's ulitmate profile [34], expressed by equation (9) with the constants $A = 11.7$ and $B = -17$. In the core region a parallel shift of the velocity profile is observed

$$U^+ = A \ln y^+ + B + \Delta B \tag{10}$$

where ΔB increases with increasing drag-reduction until in the case of Virk's maximum drag-reduction the turbulent core region vanishes due to the expanded buffer zone. In Eq. (6) usually the solvent viscosity is used. This may cause problems, when drag-reducing fluids with a strongly shear-dependent viscosity are used. It will be discussed in detail later on for the velocity profiles of the C_{16}TASal solution.
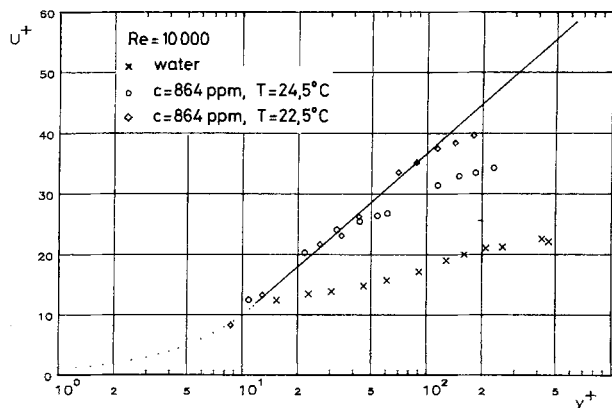
Fig. 10. Dimensionless velocity profile of a C_{14}TASal solution at different temperatures at $Re = 10\,000$
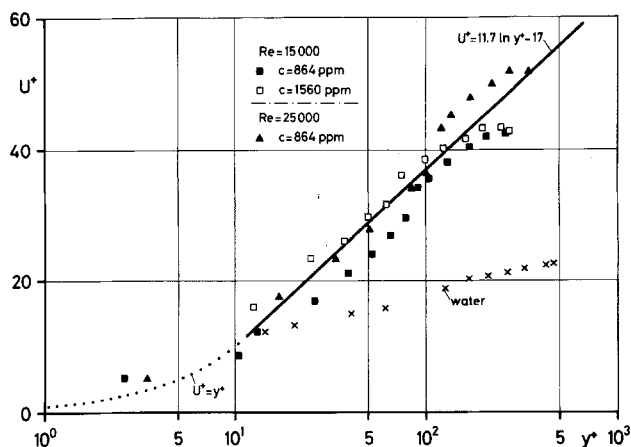

Fig. 11. Dimensionless velocity profile of a C_{14}TASal solution at $T = 23\,°C$ for different Reynolds numbers and surfactant concentrations

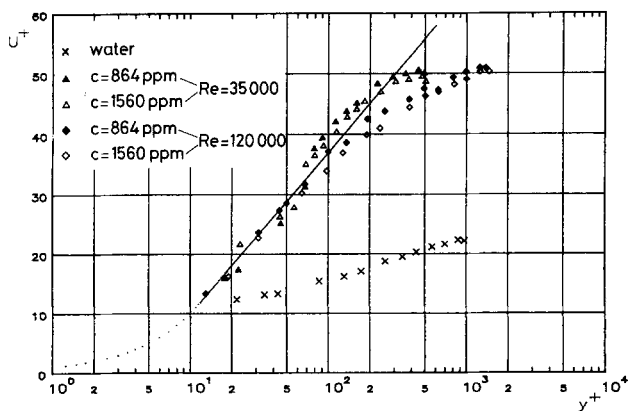

Fig. 12. Dimensionless velocity profile of a C_{14}TASal solution at $T = 23\,°C$ for different Reynolds numbers and surfactant concentrations

The results of the velocity profile measurements of the C_{14}TASal solution are presented in Figs. 10–12. Figure 10 shows turbulent velocity profiles of the surfactant solution at a Reynolds number of 10^4 for different temperatures. As expected from the friction behaviour (see chapter 3.2) the velocity profiles strongly depend on the temperature. From the end of the viscous sublayer the velocity profiles first follow Virk's ultimate profile (straight line) before they deviate to a core region at a certain wall distance. In the core region the slope of the velocity profile is slightly increased in comparison with that of the solvent. With increasing drag reduction obtained by a change in temperature, the buffer zone expands. When the Reynolds number is increased and the friction factor approaches (region 2) Virk's maximum drag-reduction asymptote (Fig. 8) the dimensionless velocity profiles become more S-shaped (Fig. 11) and only a small core region is detectable ($Re = 15\,000$). In a certain wall distance region, the data lie between Virk's ultimate profile and the curve of a laminar profile ($Re = 25\,000$). This effect becomes more distinct at a Reynolds number of $35\,000$ (Fig. 12) at maximum drag-reduction conditions. In this case the concentration has only a neglectable influence on the shape of the velocity profile. A further increase of the Reynolds number to $120\,000$ where the friction factor is nearly independent of the Reynolds number (region 3) exhibits the formation of a core region. Virk's ultimate profile is again a good approximation of the velocity profile in the buffer zone, whereas in the core region a conspicuous increase in the slope of the velocity profile in comparison to that of the solvent occurs. This is in contrast to the behaviour of dilute polymer solutions where a parallel shift of the velocity profile in the core region is observed indicating no change in the turbulence structure in comparison with that of the solvent.

The S-shaped velocity profiles at maximum drag-reduction conditions were also observed in [36–38] where a solution of the surfactant Methaupon was studied. Figure 13 contains data of the turbulent velocity profiles from [37], obtained in a channel flow at different pressure drops and surfactant concentrations. Subject to these parameters, velocity profiles can be found which look quite similar to those of the present work.

Due to the complex rheological behaviour of the C_{16}TASal solution the question arises which viscosity should be used for calculating the dimensionless wall distance y^+ in the velocity profiles. The different methods applied for calculating y^+ can be seen in
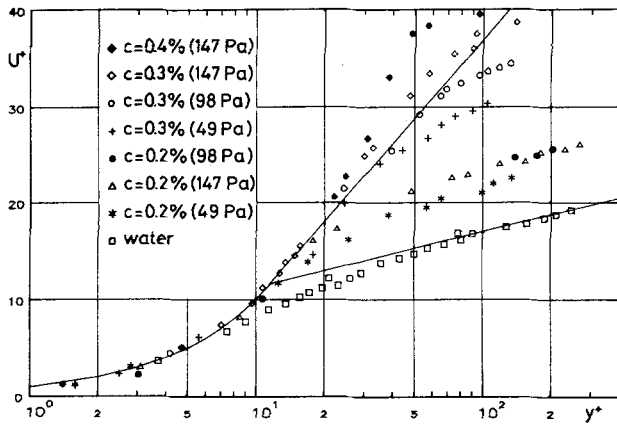
Fig. 13. Dimensionless velocity profiles for different concentrations of the surfactant Methaupon at different pressure drops from [36] obtained in a rectangular channel (20 × 50 mm)

Fig. 15. Dimensionless velocity profiles of a $C_{16}TASal$ solution at $T = 25\,°C$ and $c = 830\,ppm$ for different Reynolds numbers. y^+ is calculated with the solution viscosity which varies with the wall distance

Fig. 14. One method is to derive the velocity profile and estimate the local velocity gradient

$$D = \frac{dU^+}{dy^+}\frac{u_\tau^2}{v_s}. \tag{11}$$

The shear viscosity for each D is taken from the flow curve (Fig. 2) where v_s means the solvent viscosity. In this way dimensionless velocity profiles are obtained that look quite similar (variable viscosity in Fig. 14) to those found in the $C_{14}TASal$ solution (in region 1). This velocity profile follows Virk's ultimate profile in the buffer zone and exhibits a core region. Therefore the
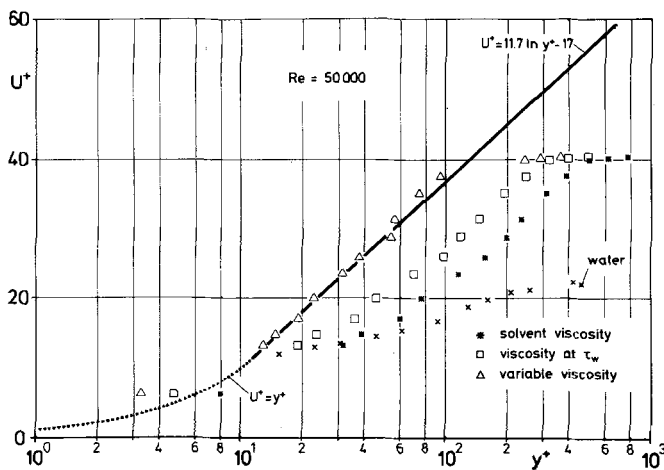
method for calculating y^+ was also used for the velocity profiles of the $C_{16}TASal$ solution at other Reynolds numbers (Fig. 15). At $Re = 25\,000$ the velocity profile shows only a small buffer zone and an increased slope in the core region similar to that of the $C_{14}TASal$ solution in region 1, whereas at $Re = 120\,000$ a S-shaped velocity profile around Virk's ulitmate profile is obtained which resembles that of the $C_{14}TASal$ solution at maximum drag-reduction conditions (Figs. 11 and 12). This indicates that the shear viscosity is mainly influenced by the mean velocity profile and not by the turbulent eddy motion.

3.4 Axial turbulence intensities

The measured axial turbulence intensities were normalized with friction velocity u_τ. In Newtonian fluids the axial turbulence intensity increases rapidly from zero at the wall to its maximum at $y^+ \approx 12$–13. From its maximum it decreases slowly towards the centre of the pipe. In drag-reducing fluids the maximum axial turbulence intensity is shifted with increasing drag-reduction to higher y^+ values. Conflicting results exist for both decreases and increases [46].

From Fig. 16 a similar behaviour of the axial turbulence intensity in drag-reducing surfactant solutions can be deduced. The maximum of the axial turbulence intensity is shifted to $y^+ \approx 100$ at $Re = 35\,000$ and to $y^+ \approx 250$ at $Re = 120\,000$ in surfactant solutions. In addition, the axial turbulence intensity seems to be increased over the whole cross section of the pipe. In comparison with literature data, the axial turbulence

Fig. 14. Dimensionless velocity profile of a $C_{16}TASal$ solution at $T = 25\,°C$ and $c = 830\,ppm$ when different shear viscosities are used for calculating y^+

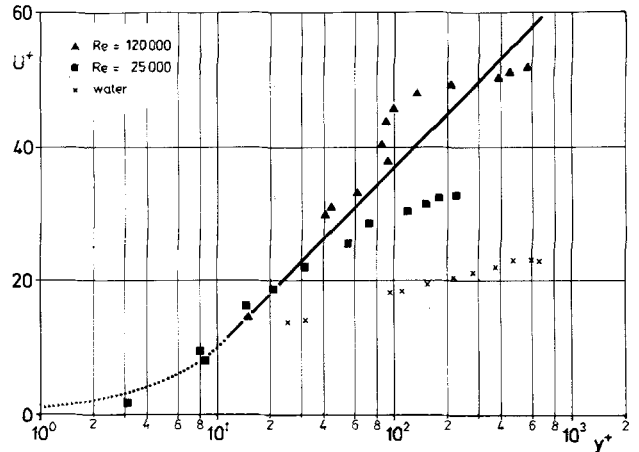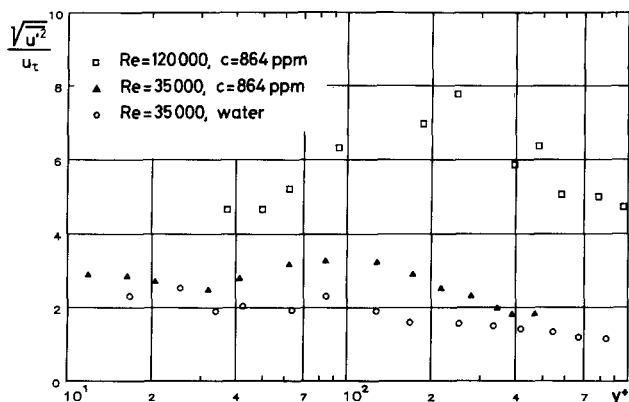Fig. 16. Axial turbulence intensities of a C_{14}TASal solution at different Reynolds numbers

intensity of the solvent (water) at $Re = 120\,000$ also exhibits a small increase, which may be due to the increased noise or size of the measuring volume of the LDA.

The autocorrelation function of the axial velocity fluctuations was estimated. In these measurements 4096 data were taken at a sample frequency of 500 Hz. The autocorrelation functions were normalized using the local axial turbulence intensities $\overline{u'^2}$. The normalized autocorrelation coefficient $R_{11}(\tau)$ is defined by

$$R_{11}(\tau) = \frac{\overline{u'(t)\,u'(t+\tau)}}{\overline{u'^2}} \qquad (12)$$

where τ means the time delay. Instead of carrying out a frequency analysis, the autocorrelation coefficient $R_{11}(\tau)$ was integrated up to a time τ_0 at which $R_{11}(\tau)$ was nearly zero.[1]) In this way an average correlation time (integral scale) was estimated as

$$T = \int_0^{\tau_0} R_{11}(\tau)\,d\tau. \qquad (13)$$

This should be understood as a measure of the macroscale of the turbulence, as suggested by Taylor. The microscale of the turbulence can also be determined from the curvature of the autocorrelation coefficient at $\tau = 0$.

The estimated macroscales and microscales in the flow of water or in a C_{14}TASal solution at $Re = 20\,000$ are shown in Figs. 17 and 18. The microscale of the sur-

factant solution is increased over the whole cross section of the pipe especially in the region near the wall. This could be interpretated as an increase in the size of the eddies in the dissipation range caused by an increased local effective viscosity. Furthermore, the integral scale seems to be increased in the flow of the surfactant solution over the whole cross section of the pipe. This means that the large-scale structure is also affected in the flow of drag reducing surfactant solutions. This agrees with the findings of [13], concluded from an analysis of the higher moments of turbulence, the distribution of the Reynolds shear stresses, and the joint density probability function.

4. Conclusions

Drag-reduction in surfactant solutions is only attainable when rod-like micelles are present in the solution [7, 23]. In a surfactant solution at rest these rod-like micelles are oriented statistically [35], i.e., meaning they have no preferred orientation. For the surfactant C_{14}TASal in equimolar mixture with the salt NaBr in tap water, the length of the rods is 50–80 nm depending on the temperature (Fig. 1), whereas the diameter of the rods is about 3.5 nm as estimated by small-angle-neutron scattering [35]. Therefore at concentrations of about 1000 ppm or lower, as used in the present investigation, the micelles may rotate freely in a shear flow without hindering each other since the rotational volumes do not overlap. This is true in laminar Couette flows at low shear gradients, where the viscosity is low and appears to be Newtonian. However, when a critical shear gradient is exceeded, the micelles start to orient until they become completely aligned in the direction of the flow. The shear viscosity then suddenly increases and ordered structures are formed. The size of these ordered structures is much larger than the length of individual rods. One concludes this from the increased shear viscosity. A further hint is that in some surfactant systems the viscosity measured in a Couette viscometer depends on the gap width [7]. In the present work for the C_{16}TASal solution the cylinder moved elliptically in the gap so that no steady values of the torque could be obtained. Therefore the size of the ordered structures seems to reach the order of the gap width of the viscometer during the shear-induced state (SIS). On the other hand, when the rods were aligned in the direction of the flow without ordered structures, the shear viscosity should decrease due to the alignment of the rods in the direction of the flow.

---

[1]) Because of the noise, the autocorrelation coefficient fluctuates around zero for large values of τ.
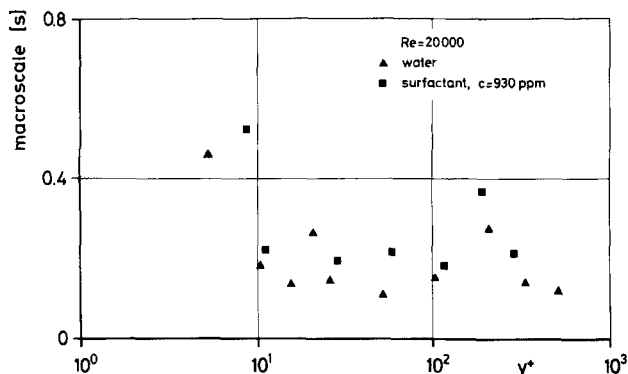
Fig. 17. Integral macroscale of the axial velocity fluctuations for water and a C_{14}TASal solution at $Re = 20\,000$ as a function of the dimensionless wall distance y^+
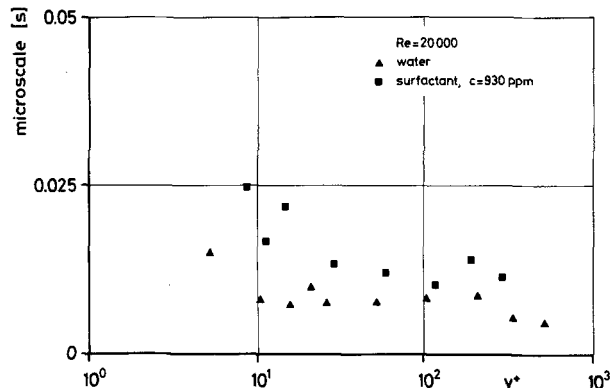

Fig. 18. Microscale of the axial velocity fluctuations for water and a C_{14}TASal solution at $Re = 20\,000$ as a function of the dimensionless wall distance y^+

In the SIS the surfactant solutions become viscoelastic. As shown in [47], surfactant solutions exhibit a larger elongational viscosity than the solvent only when they are presheared. In these experiments [47], the solutions were first subjected to a laminar shear gradient in a channel flow before they entered an elongational field produced by a hole in the wall. Only when a critical shear rate was exceeded, did the elongational viscosity start to increase. This helps one to understand the behaviour of these solutions in turbulent-shear flows, where elongational fields occur in the movement of coherent structures, the so-called "bursts", in the region near the wall. Note that the elongation does not commence during the burst out of an equilibrium state. The micelles are in fact already subjected to a shear flow near the wall before they experience the additional elongational field of the burst. Therefore a better understanding of drag-reduction in surfactant solutions requires not only the knowledge of the shear viscosity as a function of the shear rate but also the knowledge of the elongational viscosity as a function of the elongational and shear rates.

The length of the rods (Fig. 1) as determined by electrical birefringence measurements increases with the salt concentration and the surfactant concentration [7, 23] but decreases with the temperature. Because of the temperature dependence of the rod lengths, the onset of the SIS is shifted to higher shear rates with increasing temperature since shorter rods shift the onset of the SIS to higher shear rates. A comparison of the friction behaviour of the C_{14}TASal solution in deionized water and in tap water (Figs. 5 and 6) makes evident that an increase in ionic strength acts like an increase in temperature. The same can be concluded from the behaviour of the shear viscosity (Figs. 3 and 4).

At low temperatures the C_{14}TASal solution causes drag-reduction in turbulent flows only when a certain critical wall-shear stress is exceeded (Fig. 5). This onset phenomenon is well known in the friction behaviour of dilute polymer solutions [34]. The viscoelastic behaviour of dilute polymeric solutions, like poly(ethylenoxide) in water [48, 49], is similar to that of drag-reducing surfactant solutions [47] in that the elongational viscosity is only increased when a critical shear rate is exceeded. At higher temperatures the critical shear rate for the C_{14}TASal solution is already exceeded in the laminar flow region so that drag-reduction occurs directly when the flow becomes turbulent. Note that the critical shear rate for SIS increases with temperature, whereas the wall-shear gradient at the laminar turbulent transition point decreases with temperature. The same friction behaviour is found for high-molecular-weight polymeric solutions in pipes of small diameters.

Dimensionless turbulent velocity profiles at low Reynolds numbers, where the friction factor falls linearly with Reynolds number (region 1 in Fig. 8), look quite similar to those found for drag-reducing dilute polymer solutions. The velocity profile and the axial turbulence intensity distribution are mainly influenced in the buffer zone close to the wall. Virk's three layer model [34] appears to be a good description of the velocity profiles in this region (Fig. 8) of the friction behaviour. The microscales estimated from the autocorrelation function of the axial velocity fluctuations exhibit the most significant increase in comparison

with the solvent in the buffer zone (Fig. 18) whereas in the core region the increase of the microscale is not so significant. This can be interpreted as an enlargement of the smallest dissipating eddies. A possible explanation is based on the increased effective viscosity [50–52]. From this reasoning the effective viscosity should show a maximum in the buffer layer and decline in the core region. This is in agreement with the findings in [50] where the behaviour of the effective viscosity was found from Reynolds shear stress measurements in the flow of drag-reducing polymeric solutions.

When the friction factor approaches Virk's [34] maximum drag-reduction asymptote, region 2 (Fig. 8), deviations from Virk's ultimate profile in the buffer zone are observed. The velocity profiles become more S-shaped, i.e., they show deviations from Virk's ultimate logarithmic profile, namely at lower wall distances to lower and in the medium range to higher dimensionless velocity values, whereas in the centre of the profile a small core region seems to exist, in agreement with earlier findings [36]. Therefore the shape of the dimensionless velocity profile at maximum drag-reduction conditions is more similar to a laminar than to a turbulent logarithmic profile. Possible explanations for these observed deviations in the velocity profile from Virk's ultimate profile could be either a pseudo-laminar velocity profile of a fluid with an effective viscosity which increases with wall distance in the buffer layer [50] or an enhanced large scale motion [53]. However, the integral scales of the autocorrelation function of the axial velocity fluctuations, which give information about the large scale motion of turbulence, exhibit only a small increase (Fig. 18). Nevertheless in region 3 (Fig. 8) of the friction behaviour the velocity profiles show an increased slope in the core region, an indication of a changed large-scale structure.

A proper method for calculating the dimensionless wall distance y^+ for drag-reducing fluids with larger shear viscosity than the solvent starts with the derivative of the velocity profile with respect to the wall distance. For every value of the velocity gradient, the viscosity measured in a viscometer then should be used for calculating y^+. In this way the velocity profiles of the C_{16}TASal solution become very similar to those found for the C_{14}TASal solution. This is a strong indication that the shear viscosity in turbulent flows of drag-reducing fluids is mainly influenced by the local mean velocity gradient. By comparison the turbulent eddy motion has a smaller influence.

At the critical wall-shear stress the superordered structures are destroyed [35] and the rod-like micelles

start to rotate in the turbulent shear flow. However, the micelles are not destroyed because when the flow-rate is decreased the drag-reduction is recovered without delay whereas the time constants involved in the formation of rod-like micelles for the surfactants used in the present investigation are on the order of 10^3–10^4 s.

References

1. Mysels KJ (1949) US Patent 2 492 173
2. Shenoy AV (1984) Colloid Polym Sci 262:319
3. Sellin RHJ, Hoyt JW, Pollert J, Scriverner O (1982) J Hydraulic Res 20:235
4. Motier JF, Prilutski DJ (1984) Third Intern Conf on Drag Reduction, Bristol, UK, paper F2
5. Sellin RHJ (1984) Third Intern Conf on Drag Reduction, Bristol, UK, paper I3
6. Zakin JL, Lui HL (1983) Chem Eng Commun 23:77
7. Ohlendorf D, Interthal W, Hoffmann H (1986) Rheol Acta 25:468
8. Myska J, Slanec K (1980) Acta Polytechnica 11:57
9. Ohlendorf D, Interthal W, Hoffmann H (1984) IX Intern Congr on Rheology, Mexico, 2:41, Elsevier Sci Publ, Amsterdam
10. Savins JG (1967) Rheol Acta 6:323
11. Elson TP, Garside J (1983) J Non-Newtonian Fluid Mech 12:121
12. Wells CS (1969) In: White A (ed) Viscous Drag Reduction. Plenum Press, New York, 297
13. Bewersdorff HW, Ohlendorf D (1985) Proc Fifth Symposium on Turbulent Shear Flows, Ithaca, New York 9:41
14. Zakin JL, Chiang JL (1974) Intern Conf on Drag Reduction, Cambridge, UK, paper D1
15. Zakin JL, Poreh M, Brosh A, Warshavsky M (1971) AIChE J Chem Engg Prog Symp Series No 111, 67:85
16. White A (1967) Nature 214:585
17. Myska J, Vocel J (1977) Chem Eng Sci 32:593
18. Povkh IL, Serdyuk AI, Naumov AV, Kovalenko NP (1980) J Engng Phys 38:639
19. Teot AS, Rose GD, Stevens GA (1986) European Patent 0092 581
20. Ohlendorf D, Hoffmann H, Interthal W, Pintschovius U (1987) European Patent 0097 926
21. Ohlendorf D, Interthal W, Barthelt H, Hoffmann H (1987) European Patent 0149 172 A1
22. Ohlendorf D, Hofinger M (1988) European Patent 0146 097 A1
23. Ohlendorf D, Interthal W (1986) In: Mittal KL, Bothorel P (eds) Surfactants in Solution. Plenum Press, New York 6:1589
24. Rehage H, Wunderlich I, Hoffmann H (1986) Progr Colloid Polym Sci 72:51
25. Löbl M, Thurn H, Hoffmann H (1984) Ber Bunsenges Phys Chem 88:1102
26. Ulmius J, Wennerström H, Johannson LBA, Lindblom G, Gravsholt S (1979) J Phys Chem 83:2232
27. Hoffmann H, Platz G, Rehage H, Schorr W, Ulbricht W (1980) Ber Bunsenges Phys Chem 85:2255
28. Gravsholt S (1976) J Colloid Interface Sci 57:575
29. Rehage H, Hoffmann H (1982) Rheol Acta 21:561
30. Rehage H, Hoffmann H (1983) Faraday Discuss Chem Soc 76:0

31. Hoffmann H, Rehage H, Thurn H, Ohlendorf D (1984) IX Intern Congr on Rheology, Mexico, 2:31, Elsevier Sci Publ, Amsterdam
32. White A (1976) Drag Reduction by Additives, BHRA Fluid Engineering
33. Zakin JL (1971) Nature Phys Sci 235:97
34. Virk PS (1975) AIChE J 21:625
35. Bewersdorff HW, Frings B, Lindner P, Oberthür RC (1986) Rheol Acta 25:642
36. Povkh IL, Stupin AB, Maksjutenko SN, Aslanov PV, Simonenko AP (1980) Mekh Turbul Potokov (Tr Vses Konf) pp 44–69
37. Aslanov PV, Maksjutenko SN, Povkh IL, Simonenko AP, Stupin AB (1980) Izv Akad Nauk SSR, Mekh Zhidk Gaza pp 36–43
38. Povkh IL, Stupin AB, Maksjutenko SN, Aslanov PV, Roshchin EA, Tur AN (1975) Inzh Fiz Zh 29:522
39. Schorr W, Hoffmann H (1981) J Phys Chem 85:3160
40. Hoffmann H, Schorr W (1985) Ber Bunsenges Phys Chem 89:538
41. Bewersdorff HW (1984) Rheol Acta 23:522
42. Hoffmann H, Platz G, Rehage H, Schorr W (1982) Advances in Colloid and Interface Science 17:275
43. Bayer O, Hoffmann H, Ulbricht W, Thurn H (1986) Advances in Colloid and Interface Science 26:177
44. Hoffmann H, Löbl H, Rehage H, Wunderlich I (to be published)
45. Ohlendorf D, Hoffmann H (to be published)
46. Berman NS (1978) Ann Rev Fluid Mech 10:47
47. Wunderlich AM, James DF (1987) Rheol Acta 26:522
48. James DF, McLean BD, Saringer JH (1987) J Rheol 31:453
49. Vißmann K (17–20 June 1986) 2nd Conf European Rheologists, Prague, CSSR (in print)
50. Bewersdorff HW, Berman NS (1988) Rheol Acta 27:130
51. Lumley JL (1969) Ann Rev Fluid Mech 1:367
52. Lumley JL (1977) Phys Fluids 20:S564
53. Long RR, Chen TC (1981) J Fluid Mech 105:19

Authors' address:

Dr. H.W. Bewersdorff
Universität Dortmund
Fachbereich Chemietechnik
Postfach 50 05 00
D-4600 Dortmund 50, F.R.G.